Urbani, S., Acocella, V., Rivalta, E. (2018): What drives the lateral versus vertical propagation of dikes? Insights from analogue models. - *Journal of Geophysical Research*, *123*, 5, pp. 3680—3697.

DOI: http://doi.org/10.1029/2017JB015376

Journal of Geophysical Research: Solid Earth

RESEARCH ARTICLE
10.1029/2017JB015376

What Drives the Lateral Versus Vertical Propagation of Dikes? Insights From Analogue Models

S. Urbani[1], V. Acocella[1], and E. Rivalta[2]

[1]Dipartimento di Scienze, Università Roma Tre, Rome, Italy, [2]Deutsches GeoForschungsZentrum GFZ, Potsdam, Germany

Key Points:
- Understanding what drives the propagation direction of dikes is a crucial step for eruption forecasting
- Analogue models show that rigidity layering (stiff layer above a soft layer) and topography dominantly favor lateral dike propagation
- A stiff layer promotes lateral propagation more efficiently than the Level of Neutral Buoyancy (LNB) by inhibiting its vertical ascent

Supporting Information:
- Supporting Information S1

Correspondence to:
S. Urbani,
stefano.urbani@uniroma3.it

Citation:
Urbani, S., Acocella, V., & Rivalta, E. (2018). What drives the lateral versus vertical propagation of dikes? Insights from analogue models. *Journal of Geophysical Research: Solid Earth*, *123*, 3680–3697. https://doi.org/10.1029/2017JB015376

Received 20 DEC 2017
Accepted 29 APR 2018
Accepted article online 5 MAY 2018
Published online 30 MAY 2018

Abstract Volcanic eruptions are usually fed by dikes. Understanding how crustal inhomogeneities and topographic loads control the direction (lateral/vertical) and extent (propagation/arrest) of dikes is crucial to forecast the opening of a vent. Many factors, including buoyancy, crustal layering, and topography, may control the vertical or lateral propagation of a dike. To define a hierarchy between these factors, we have conducted analogue models, injecting water (magma analogue) within gelatin (crust analogue). We investigate the effect of crustal layering (both rigidity and density layering), topography, magma inflow rate, and the density ratio between host rock and magma. Based on the experimental observations and scaling considerations, we suggest that rigidity layering (a stiffer layer overlying a weaker one) and topographic gradient favor predominantly lateral dike propagation; inflow rate, density layering, and density ratio play a subordinate role. Conversely, a softer layer overlying a stiffer one favors vertical propagation. Our results highlight the higher efficiency of a stiff layer in driving lateral dike propagation and/or inhibiting vertical propagation with respect to the Level of Neutral Buoyancy proposed by previous studies.

1. Introduction

Understanding dike propagation and emplacement is crucial to define magma transfer and extrusion within the crust. Geological and geophysical data at volcanoes and rift zones reveal that dikes expand and propagate in all directions but tend to propagate mostly laterally or vertically.

Laterally propagating dikes have been recognized at many volcanic edifices such as Etna, Vesuvio, Stromboli, Kilauea, Miyakejima, Piton de La Fournaise, and El Hierro (Fukushima et al., 2005; Peltier et al., 2009; Acocella & Neri, 2009, and references therein; Martí et al., 2013; Rivalta et al., 2015). Rifting episodes along divergent plate boundaries in Afar and Iceland also highlight a predominant lateral transfer of magma along rifts (Ayele et al., 2009; Biggs et al., 2009; Ebinger et al., 2010; Einarsson & Brandsdóttir, 1980; Nobile et al., 2012; Sigmundsson et al., 2015; Wright et al., 2012). However, dikes may also propagate vertically, both in volcanic edifices, such as Vesuvio, Etna, or Piton de la Fournaise (Acocella & Neri, 2003; Acocella et al., 2006; Battaglia et al., 2005), and along rift zones, as at Harrat Lunayyr (Pallister et al., 2010) and Iceland (Hartley & Thordarson, 2012, 2013).

Several factors may dictate whether a dike will propagate vertically or laterally. Among these, buoyancy has been proposed as the dominant control (Menand & Tait, 2002; Taisne & Tait, 2009; Takada, 1990; Townsend et al., 2017); a neutrally buoyant dike may arrest and expand laterally at the Level of Neutral Buoyancy (LNB; Lister & Kerr, 1991). Moreover, stiffer layers overlying more compliant ones may provide barriers to magma ascent (A. Gudmundsson, 2006; Kavanagh et al., 2006; Maccaferri et al., 2011; Rivalta et al., 2005). Topographic reliefs provide a driving pressure for propagation by inducing lateral stress gradients (Acocella & Neri, 2009; Fialko & Rubin, 1999; Fiske & Jackson, 1972; Kervyn et al., 2009; Maccaferri et al., 2016; Muller et al., 2001; Pinel et al., 2017; Pinel & Jaupart, 2004; Rubin & Pollard, 1987), also inducing an increasingly intense compression at the tips of ascending dikes or approaching a relief, favoring dike arrest (Kervyn et al., 2009; Maccaferri et al., 2011, 2016; Urbani et al., 2017; Watanabe et al., 2002). Additionally, reliefs modify dike trajectories by inducing rotations of the principal stress axes that may lead a dike to change propagation direction, for example, from vertical to horizontal or vice versa (Bagnardi et al., 2013; Corbi et al., 2015, 2016; Dahm, 2000; Maccaferri et al., 2014; Watanabe et al., 2002). Preexisting discontinuities in the host rock may channelize the dikes, causing their arrest or deviation (Ito & Martel, 2002; Le Corvec et al., 2013; Maccaferri et al., 2016; Watanabe et al., 2002; Ziv et al., 2000). Gradients in external stresses (e.g., rift extension) may contribute to drive dikes away from their magma reservoir (Buck et al., 2006; Grandin et al., 2012) and to their equilibrium position below the surface (i.e., the level at which vertical propagation is arrested and magma propagates laterally; Buck et al., 2006;

Townsend et al., 2017). Magma influx from the reservoir also provides a driving pressure for dike propagation (Rivalta, 2010; Taisne et al., 2011). Magma cooling (Taisne & Tait, 2011) and volatile exsolution (Menand & Tait, 2001; Taisne & Jaupart, 2011) change the rheological proprieties of magma (i.e., density and viscosity) and modify the pressure balance within dikes.

Despite this knowledge, the relative importance of these potential contributions has been not investigated so far. Defining a hierarchy between the various processes controlling vertical and lateral dike propagation would finally provide a crucial advancement in understanding how magma is transferred in the crust and within volcanic edifices. This may allow capturing the weight of the most important processes controlling magma migration and help evaluating the possibility of opening of a vent in a given area.

To define a hierarchy between the various factors, we have conducted analogue models, injecting water (magma analogue) within gelatin (crust analogue). In particular, we have investigated the control on lateral versus vertical dike propagation by the following factors: rigidity layering, density layering, density ratio between the host rock and magma analogue, the inflow rate of the magma analogue, and topography; we have then discussed our results based on scaling the experiments to nature. Previous results with the same experimental apparatus showed that the joint effect of topography and rigidity layering assists lateral propagation, with an opposing slope causing dike arrest (Urbani et al., 2017). In this work, we (1) further expand and (2) also complement those experiments with newly imposed parameters (density ratio between host rock and magma analogues, density layering, and flow rate), by varying systematically each of all the parameters and comparing semiquantitatively the variations on dike geometry and velocity, defining a hierarchy of all the parameters considered.

2. Methods

2.1. Analogue Models: Experimental Setup

We performed 33 analogue models, including the four already presented in Urbani et al. (2017) with the same experimental apparatus. Within a $33 \times 58 \times 38.5$ cm^3 plexiglass box, we injected dyed water in pig-skin gelatin as magma and crustal analogues, respectively (Di Giuseppe et al., 2009; Figure 1a). In 24 of these experiments, we created two gelatin layers, pouring gently two solutions of different gelatin and/or NaCl concentration one above the other while this was still at the liquid state. NaCl decreases gelatin rigidity and increases its density (Brizzi et al., 2016). This process generates a partial mixing of the two layers and, after cooling in the refrigerator, an ~4-cm thick nonsharp interface with a rigidity and density gradient (Urbani et al., 2017). We refer to rigidity layering when the rigidity ratio between the upper and lower layer (E_u/E_l) is $<$ or >1 and to density layering when $E_u/E_l \sim 1$, but the two layers show different densities. To investigate the role of topography ("topography" models), we imposed a mold on the gelatin surface, producing two inward dipping slopes (dip 2.4° and 3.7°, respectively) separated by an 8-cm-long flat plain (Urbani et al., 2017).

We finally injected dyed water (density ρ_f ranging from 993 to 1,116 kg/m^3) alternatively from the bottom ("vertical injection" experiments, Set 1) or the side ("horizontal injection" experiments, Set 2) of the box using a peristaltic pump with influx rate (Q) between 0.079 and 0.435 ml/s. In both Set 1 and Set 2 we inserted the needle tip parallel to the *x-z* plane (Figures 1a–1c, 2a–2d, and 4a–4d) to impose the initial dike strike parallel to that plane. If the dike strike was oblique to this plane, the dike length and breadth, which were measured from the images and thus projected on the *x-z* plane, were corrected according to the angle calculated from the top view images (β in Table 2, spanning from 0° to 55°).

Gelatin temperature was kept at 9 °C, water at 20 °C. The thickness ratio between the upper and lower layer (T_u/T_l, where T_u and T_l are the thickness of the upper and lower layer, respectively) ranges from 0.63 to 2.54 (Table 1). We monitored dike propagation alternatively in side and top view, at 0.2 and 0.1 frames per second.

We define a hierarchy among the investigated factors by quantifying how far the dikes propagate laterally under different conditions. With regard to Set 1 experiments without topography, we measure the dike breadth of each experiment 3 cm above (b_u) and below (b_l) the center of the interface; this allows us to evaluate any dike shape change (Figure 1b). We define b_u/b_l as the shape ratio of the dike. In Set 1 experiments with topography, we measure the maximum distance reached by the dike along either side from the

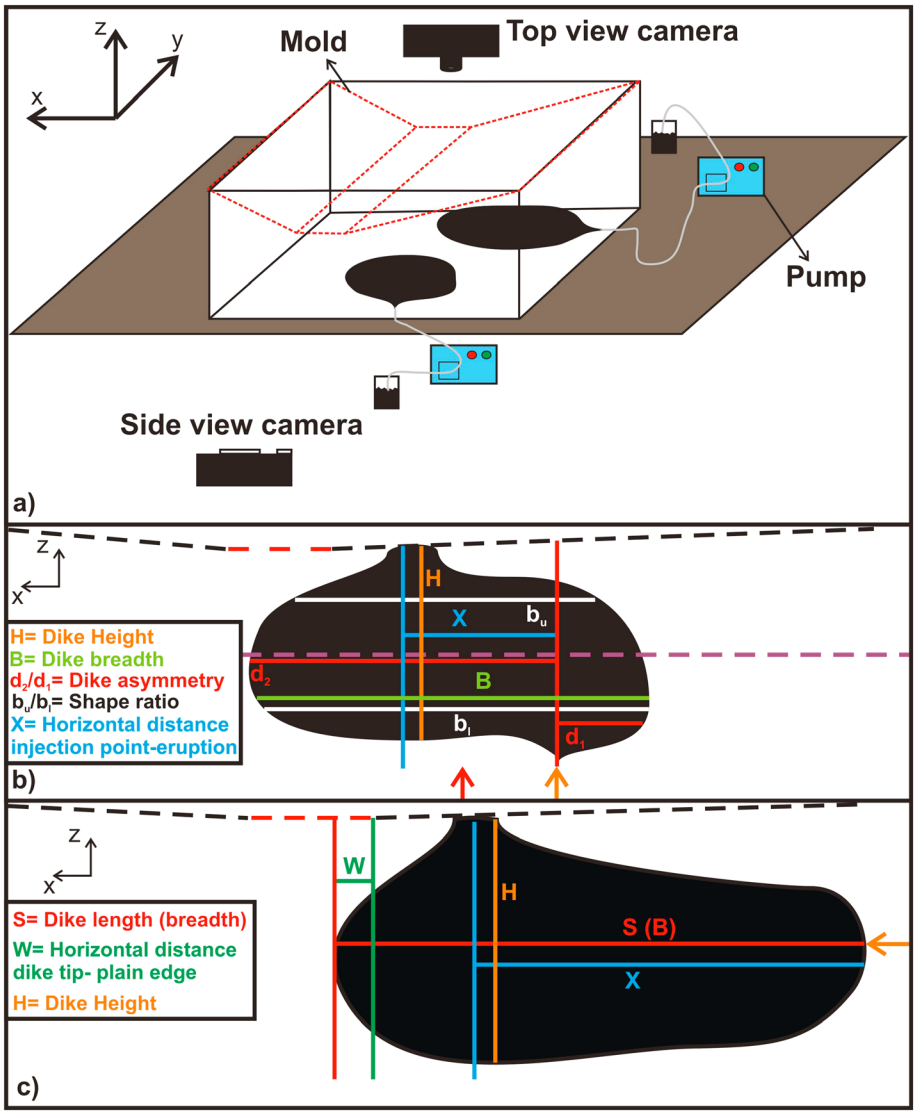

Figure 1. (a) Sketch of the experimental setup. The reference system in the top left refers to the box sides. The red dashed lines in the box represent the topography used in some experiments, while the two black dikes represent Set 1 and Set 2 experiments where injection occurred from the bottom or the side of the box, respectively. (b) Section view diagram illustrating the measurement procedure for b_l, b_u, d_1, d_2, X, B, and H in Set 1 experiments (see text for details). Red and orange arrows indicate the injection points without and with topography, respectively. The dashed black, red, and purple lines indicate the slopes, the plain and the interface center, respectively. (c) Section view measurement procedure for B, H, S (coincident with B), W, and X, Set 2. Orange arrow indicates the injection point.

injection point (d_2 and d_1 in Figure 1b), defining d_2/d_1 as dike "asymmetry." With respect to the experiments without topography, we shift the injection point 9 cm from the center to the right side, below the slope, to evaluate any dike propagation caused by the asymmetric topography. The horizontal distance between the eruption and injection points (X) is also measured (Figures 1b and 1c).

In Set 2 we measure the dike length (S, Figure 1c). Moreover, to compare the results from Set 1 and Set 2 for experiments with topography, we measure the horizontal distance between the dike tip and the plain edge (W, Figure 1c). In this case, we consider the plain edge as a reference axis: positive values indicate a dike tip below the plain (Table 2). Finally, in both Set 1 and Set 2 we measured the dike aspect ratio (Breadth/Height, B/H). All the measurements have an error of ±0.5 cm related to camera distortion. Table 1 shows the imposed parameters in each experiment. Figures S1 to S8 in the supporting information show experiments not presented extensively in the main text and/or excluded from the data set, since they replicate experiments already presented in this paper. In particular, experiments in Figure S6 (32, 33, 34, and 51) were also presented in Urbani et al. (2017; referred there as numbers 4, 1, 3, and 2, respectively).

Table 1
Imposed Parameters (and Relative Errors) in Each Experiment

Exp	ρ_L (kg/m^3)	ρ_U (kg/m^3)	ρ_f (kg/m^3)	ρ_U/ρ_f	E_l (kPa)	E_u (kPa)	E_u/E_l	T_l (cm)	T_U (cm)	T_U/T_l	Q (ml/s)
2	1,123.2	1,018.1	1,094.4	0.9303	1.8 ± 0.6	3.3 ± 0.06	1.83	9.8 ± 0.5	7.7 ± 0.5	0.79	0.079
5	1,053.6	1,018.1	1,053.6	0.9663	2.5 ± 0.2	3.3 ± 0.06	1.32	9.1 ± 0.5	9.4 ± 0.5	1.03	0.079
6	1,123.2	1,018.1	1,073.8	0.9481	1.8 ± 0.6	3.3 ± 0.06	1.83	8.7 ± 0.5	9.5 ± 0.5	1.09	0.079
8	1,071.3	1,018.1	1,116.4	0.9119	3.5 ± 0.25	3.3 ± 0.06	0.94	10.1 ± 0.5	7.3 ± 0.5	0.72	0.079
10	1,071.3	1,018.1	993.6	1.0247	3.5 ± 0.25	3.3 ± 0.06	0.94	10.1 ± 0.5	6.6 ± 0.5	0.65	0.079
11	1,071.3	1,018.1	1,053.6	0.9663	3.5 ± 0.25	3.3 ± 0.06	0.94	9.3 ± 0.5	8.4 ± 0.5	0.90	0.079
12	1,071.3	1,018.1	993.6	1.0247	3.5 ± 0.25	3.3 ± 0.06	0.94	8.9 ± 0.5	8.1 ± 0.5	0.91	0.435
13	1,053.6	1,018.1	1,053.6	0.9663	2.5 ± 0.2	3.3 ± 0.06	1.32	10 ± 0.5	7.1 ± 0.5	0.71	0.435
17	/	1,018.1	1,116.4	0.9119	/	3.3 ± 0.06	/	/	/	/	0.079
19	/	1,018.1	993.6	1.0247	/	3.3 ± 0.06	/	/	/	/	0.079
20b	/	1,018.1	1,116.4	0.9119	/	3.3 ± 0.06	/	/	/	/	0.435
21	1,071.3	1,018.1	993.6	1.0247	3.5 ± 0.25	3.3 ± 0.06	0.94	10 ± 0.5	8.5 ± 0.5	0.85	0.079
23	1,053.6	1,018.1	1,053.6	0.9663	2.5 ± 0.2	3.3 ± 0.06	1.32	10.5 ± 0.5	6.6 ± 0.5	0.63	0.079
24	/	1,018.1	1,053.6	0.9663	/	3.3 ± 0.06	/	/	/	/	0.079
26	1,069.3	1,018.1	1,053.6	0.9663	7 ± 0.38	3.3 ± 0.06	0.47	10.3 ± 0.5	7.5 ± 0.5	0.73	0.079
27	/	1,018.1	993.6	1.0247	/	3.3 ± 0.06	/	/	/	/	0.079
28	1,123.2	1,018.1	1,073.8	0.9481	1.8 ± 0.6	3.3 ± 0.06	1.83	9.5 ± 0.5	8.6 ± 0.5	0.91	0.079
29	/	1,018.1	1,116.4	0.9119	/	3.3 ± 0.06	/	/	/	/	0.079
30	/	1,088	1,008.8	1	/	3.3 ± 0.06	/	/	/	/	0.079
32	1,053.6	1,018.1	1,053.6	0.9663	2.5 ± 0.2	3.3 ± 0.06	1.32	10.3 ± 0.5	8.2 ± 0.5	0.80	0.079
33	1,071.3	1,018.1	1,053.6	0.9663	3.5 ± 0.25	3.3 ± 0.06	0.94	10 ± 0.5	7.5 ± 0.5	0.75	0.079
33b	1,071.3	1,018.1	1,116.4	0.9119	3.5 ± 0.25	3.3 ± 0.06	0.94	10 ± 0.5	7.5 ± 0.5	0.75	0.079
34	1,071.3	1,018.1	1,053.6	0.9663	3.5 ± 0.25	3.3 ± 0.06	0.94	10 ± 0.5	8.2 ± 0.5	0.82	0.079
36	1,053.6	1,018.1	1,053.6	0.9663	2.5 ± 0.2	3.3 ± 0.06	1.32	/	/	/	0.079
39	/	1,018.1	1,116.4	0.9119	/	3.3 ± 0.06	/	/	/	/	0.435
51	1,053.6	1,018.1	1,053.6	0.9663	2.5 ± 0.2	3.3 ± 0.06	1.32	9.5 ± 0.5	7.9 ± 0.5	0.83	0.079
51b	1,053.6	1,018.1	1,053.6	0.9663	2.5 ± 0.2	3.3 ± 0.06	1.32	9.5 ± 0.5	7.9 ± 0.5	0.83	0.435
52	1,071.3	1,018.1	993.6	1.0247	3.5 ± 0.25	3.3 ± 0.06	0.94	9.8 ± 0.5	7.5 ± 0.5	0.77	0.079
52b	1,071.3	1,018.1	993.6	1.0247	3.5 ± 0.25	3.3 ± 0.06	0.94	9.8 ± 0.5	7.5 ± 0.5	0.77	0.435
53	1,071.3	1,018.1	993.6	1.0247	3.5 ± 0.25	3.3 ± 0.06	0.94	9.8 ± 0.5	9.7 ± 0.5	0.99	0.079
57	/	1,018.1	993.6	1.0247	/	3.3 ± 0.06	/	/	/	/	0.079
60	1,010	1,003	993.6	1.0095	13 ± 0.54	2.5 ± 0.04	0.19	10 ± 0.5	6.6 ± 0.5	0.66	0.079
61	1,071.3	1,018.1	1,053.6	0.9663	3.5 ± 0.25	3.3 ± 0.06	0.94	6.1 ± 0.5	15.5 ± 0.5	2.54	0.079

Note. ρ_L = lower layer density; ρ_U = upper layer density; ρ_f = water density; ρ_U/ρ_f = density ratio; E_l = lower layer rigidity; E_u = upper layer rigidity; E_u/E_l = rigidity ratio; T_l = lower layer thickness; T_u = upper layer thickness; Q = flow rate. The Young's modulus values of the gelatin are from Ritter (2012). Set 1 and Set 2 experiments are indicated in red and blue respectively.

2.2. Scaling

Fluid injections in gelatin offer well-scaled analogs of magma injections into brittle-elastic rock, as summarized by Kavanagh et al. (2013), reporting scaling of lengths, time and pressures that we recalculate for parameters used here as $L^* = 1.9 \times 10^{-5}$, $T^* = 2.6 \times 10^{-3}$, $p^* = 1.9 \times 10^{-7}$ (asterisk indicates ratio of values between models and nature). Here we additionally check that the scaling of the imposed thickness of the layers and dike lengths, controlled by lateral pressure gradients in the experiments with topography, matches with the vertical dike length scales defined above. Dike height scales in our experiments as H^* = 21 cm/8 km = 2.6×10^{-5}, similar to L^*. Our upper layer thickness scales as follows: T_u^* = 7.3–15.5 cm/3 km = 2.4–5.2×10^{-5}, which is similar to, or larger than L*, implying that our upper layers are well scaled in some experiments or quite thick in others.

The horizontal dike length below a topographic slope (L_s) is controlled by the horizontal pressure gradient of the slope:

$$L_s = [K_c/\rho_r g\,(\Delta h/L)]^{2/3} \quad (1)$$

where K_c is the fracture toughness, ρ_r is the density of the host medium, g is gravity, and Δh and L are the slope height and length, respectively. We used $K_c = 10^9$ Pa m$^{1/2}$, ρ_r = 2,800 kg/m^3, g = 9.8 m/s, Δh = 700 m, and $L = 30 \times 10^3$ m for nature (as for Bardarbunga) and K_c = 83 Pa m$^{1/2}$, ρ_r = 1,000 kg/m^3, g = 9.8 m/s^2, $\Delta h = 1.3 \times 10^{-2}$ m, and $L = 35 \times 10^{-2}$ m for the laboratory, obtaining $L_s^* = 2.67 \times 10^{-5}$. This is consistent with L^*, demonstrating that our slopes are scaled.

Table 2
Measured Features in Each Experiment

Exp	β	b_u/b_l	d_2/d_1	B/H	X (cm)	S (cm)	W (cm)	Figure
2	52°	0	/	2.73	/	/	/	/
5	17°	0.91	/	1.62	/	/	/	2a
6	27°	0	/	3.20	/	/	/	S4a
8	20°	0.83	/	0.88	/	/	/	S4b
10	16°	1.04	/	0.72	/	/	/	S4c
11	43°	0.86	/	0.79	/	/	/	2b
12	0°	0.86	/	0.72	/	/	/	S7a
13	55°	0.66	/	1.33	/	/	/	S7b
17	30°	/	2.2	1.45	4.7 ± 0.5	/	4.6 ± 0.5	S2a
19	32°	/	1.93	0.78	0	/	−5.2 ± 0.5	S2b
20b	0°	/	1.79	1.78	/	/	4.3 ± 0.5	S2d
21	0°	1.66	4.3	0.78	3.1 ± 0.5	/	−3.9 ± 0.5	2d
23	20°	0.63	6.48	1.25	9 ± 0.5	/	5.3 ± 0.5	2c
24	23°	/	2.31	1.07	5.7 ± 0.5	/	2.6 ± 0.5	S2c
26	41°	1.14	/	0.53	/	/	/	S1a
27	0°	/	/	0.83	5.9 ± 0.5	11.7 ± 0.5	/	4a
28	10°	0	/	9.27	/	53.3 ± 0.5	/	/
29	15°	/	/	0.86	/	9 ± 0.5	−21.5 ± 0.5	4c
30	0°	/	/	1.13	9.5 ± 0.5	16.6 ± 0.5	−14.7 ± 0.5	4b
32	18°	/	/	2.32	22.8 ± 0.5	33.8 ± 0.5	3.3 ± 0.5	S6d
33	5°	1.45	/	0.81	4.2 ± 0.5	8.5 ± 0.5	/	S6a
33b	6°	1.73	/	0.78	4.3 ± 0.5	8.4 ± 0.5	/	/
34	17°	1.52	/	0.85	4.8 ± 0.5	9.1 ± 0.5	−20.7 ± 0.5	S6c
36	26°	/	/	1.75	20.1 ± 0.5	28.7 ± 0.5	−2.5 ± 0.5	4d and S3a
39	19°	/	/	1.06	/	12.4 ± 0.5	−17.5 ± 0.5	S5a
51	0°	/	/	1.45	11 ± 0.5	21.3 ± 0.5	/	S6b
51b	30°	/	/	1.39	11.3 ± 0.5	22 ± 0.5	/	/
52	11°	/	/	0.94	4.6 ± 0.5	9.3 ± 0.5	/	S5b
52b	0°	/	/	0.86	3.9 ± 0.5	8.9 ± 0.5	/	S5b
53	10°	/	/	0.93	5.7 ± 0.5	10.4 ± 0.5	−23.5 ± 0.5	S5c
57	20°	/	/	0.99	/	/	/	S4d
60	0°	0.78	/	0.60	/	/	/	S1b
61	15°	1.18	/	1	/	/	/	S8

Note. β = angle between dike strike and *x*-*z* plane; b_u/b_l = shape ratio; d_2/d_1 = dike asymmetry; B/H = Dike aspect ratio (Breadth/Height) X = horizontal distance between the eruption and injection points; S = dike length; W = horizontal distance dike tip-plain edge. Set 1 and Set 2 experiments are indicated in red and blue, respectively (the experiments with topography are also highlighted in bold).

Scaling of the relative importance of viscous, topographic loading and fracture pressures was presented by Urbani et al. (2017; Table S1) and Rivalta et al. (2015). The main dimensionless parameters relevant to our problem are

$$\Pi_1 = (\Delta\rho L)/(\rho_r \Delta h) \tag{2}$$

that is, the ratio between vertical ($P_{f\ \mathrm{vert}} = \Delta\rho g$) and horizontal due to a topographic load ($P_{f\ \mathrm{horiz}} = \rho_r \Delta h/L$) pressure gradient, which establishes whether the propagation is predominantly vertical or horizontal, and

$$\Pi_2 = p_v/p_f = \left[\mu^3 Q\eta/\left(Kc^4\,(1-\nu)^3\right)\right]^{1/6} \tag{3}$$

(equation (29) in Rivalta et al., 2015), which describes whether viscous pressure (p_v) dominates over fracture pressure (p_f). $\Delta\rho$ is the density difference between host medium and fluid, Q is the flow rate, η is the fluid viscosity, μ is the shear modulus, and ν the Poisson ratio. Therefore,

$$\Pi_1\ (\mathrm{models}) = 20\ \mathrm{kg/m^3}\times 0.32\ \mathrm{m}/1{,}000\ \mathrm{kg/m^3}\times 1.3\times 10^{-2}\ \mathrm{m} = 0.49$$

$$\Pi_1\ (\mathrm{nature}) = 20\ \mathrm{kg/m^3}\times 45\times 10^3\ \mathrm{m}/2{,}800\ \mathrm{kg/m^3}\times 700\ \mathrm{m} = 0.46$$

$$\Pi_2\ (\mathrm{models}) = \left[\left(1.17\times 10^3\right)^3\ \mathrm{Pa}\times 7.9\times 10^{-8}\ \mathrm{m^3/s}\times 1.2\times 10^3\ \mathrm{Pa\ s}/(83)^4\ \mathrm{Pa\ m^{1/2}}\times(0.5)^3\right]^{1/6} = 0.79$$

$$\Pi_2\ (\mathrm{nature}) = \left[\left(0.3\times 10^{11}\right)^3\ \mathrm{Pa}\times 286\ \mathrm{m^3/s}\times 10\ \mathrm{Pa\ s}/\left(10^9\right)^4\ \mathrm{Pa\ m^{1/2}}\times(0.75)^3\right]^{1/6} = 0.75$$

2.3. Experimental Limitations

In our experiments, we neglect the contribution of regional stresses (both compressional and extensional) on dike propagation, already addressed by Menand et al. (2010) and Daniels and Menand (2015). This is likely an important factor, considering also that in nature a layered crust stores different amount of stresses. For example, a weak upper layer may arrest dike ascent by not storing much extensional stress (A. Gudmundsson, 2003).

Another limitation of the experimental setup is the finite size of the gelatin layers (both horizontally and vertically) and the rigidity of the plexiglass box. Indeed, the rigid box sides force an upward propagation even in case of negative buoyancy (experiment 8). However, the rigid box does not affect significantly the stress field induced by the imposed topography (i.e., σ_3 is subhorizontal beneath the slopes and subvertical beneath the plain; Urbani et al., 2017).

A third possible limitation, discussed in Corbi et al. (2016), is the "gravitationally loaded" state of stress of the gelatin in the models with topography. This state of stress arises from the relaxation of the gelatin mass under its own weight when the mold is removed. This may not correspond to the state of stress of volcanoes and rifts in nature, due to the layer-by-layer way volcanic topography develops and to the many processes acting on volcanoes and rifts that tend to homogenize stress over time (seismicity, viscoelasticity, plasticity, and repeating dike intrusions; Chadwick & Dieterich, 1995; Corbi et al., 2015, 2016).

Several simplifications affect this study. First, we neglect solidification effects (Chanceaux & Menand, 2014, 2016; Taisne & Tait, 2011). Second, we injected a gas-free liquid, thus neglecting the effects of gas bubbles in the magma or a gas pocket below the upper dike edge, on the overall buoyancy. Considering a two-phase system (gas + liquid) with potentially inhomogeneous distribution of the volatiles over depth would add numerous complexities and require a dedicated study. Third, in order to adequately evaluate dike propagation, we assume unlimited magma availability, considering a continuous magma input inside the dike. In nature, inflow from the magma chamber into the dike usually decreases with time, changing the ratio between fracture and viscous pressure. Finally, we neglect viscosity changes in magma. Since solidification effects are negligible for high propagation rates, this assumption is adequate for modeling low-viscosity mafic lateral dikes emplaced at propagation rates between 0.2 and 20 km/hr, as at Krafla 1975–1984, Dabbahu 2005–2010, and Bardarbunga 2014–2015.

3. Results

3.1. Set 1 (Injection From the Bottom)

First, we show six representative experiments of Set 1 starting with two experiments without topography and with rigidity or density layering (experiments 5 and 11 respectively; Figures 2a and 2b), before comparing them with two similar experiments (i.e., showing rigidity and density layering) with topography (experiments 23 and 21, respectively; Figures 2c and 2d and Table 1). Table 2 lists the measured parameters in each experiment.

Rigidity layering controls the final dike shape. Increasing the rigidity ratio (from 0.47 to 1.83) leads to dikes that can hardly penetrate the upper layer (strong decrease of the shape ratio, b_u/b_l, from 1.14 to 0; Figure 3a).

Keeping the rigidity ratio constant (E_u/E_l = 0.94) and increasing the fluid buoyancy in the upper layer (i.e., increasing ρ_U/ρ_f, hereafter called density ratio, from 0.91 to 1.02) results in dike expansion in the upper layer, with b_u/b_l changing from 0.83 to 1.18 (experiments 8, 10, 11, and 61 in Figure 3b).

Increasing the flow rate (from 0.079 to 0.435 ml/s, see experiment 12 to be compared with experiment 10) while keeping density and rigidity ratio unchanged results in minor shape variations, so that b_u/b_l ranges from 1.04 (experiment 10) to 0.86 (experiment 12) and from 0.91 (experiment 5) to 0.66 (experiment 13).

Topography promotes asymmetric dikes ($d_2/d_1 > 1$; Table 2). Both density (when $E_u/E_l \sim 1$) and rigidity layering ($E_u/E_l = 1.32$), keeping the density ratio constant, increase the dike asymmetry (d_2/d_1 ranges from 1.93 and 2.31 to 4.3 and 6.28 in experiments 19, 24, 21, and 23, respectively, Figure 3c), especially with rigidity layering (experiment 23, Figure 3d).

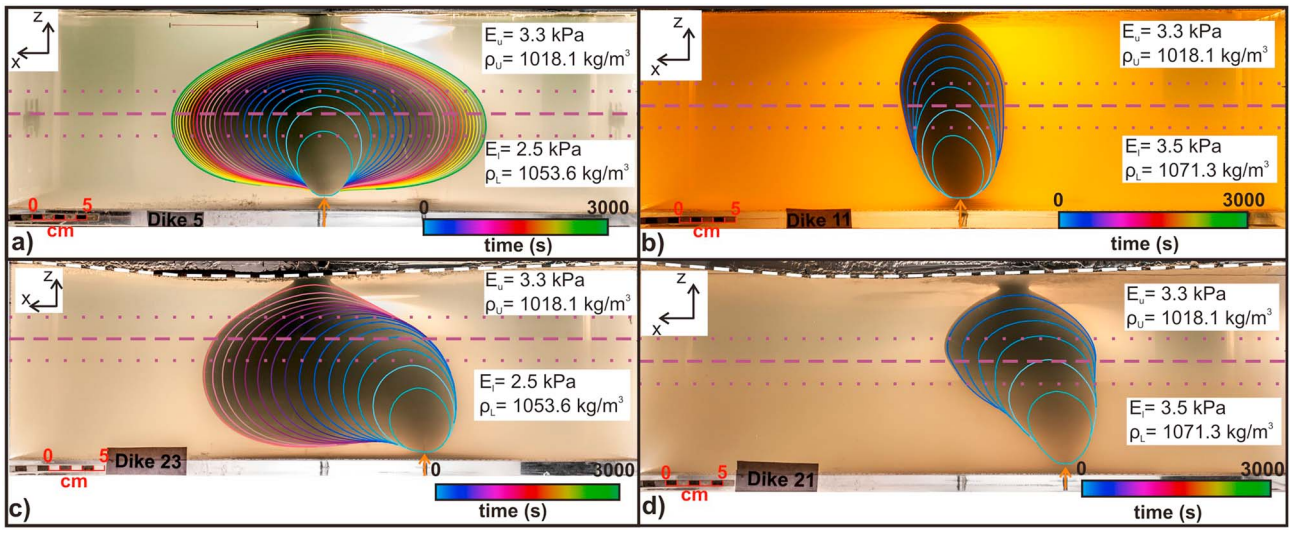

Figure 2. Section view set 1 experiments showing flat topography, rigidity (a, experiment 5), and density layering (b, experiment 11), with topography, rigidity (c, experiment 23), and density layering (d, experiment 21). The dashed purple and white lines indicate the interface center and the topography profile, respectively. The dotted purple lines indicate the limits of the interface. The reference system in the top left refers to the box sides and Figure 1a. The orange arrows indicate the injection points. The colored lines indicate the dike edge contour every 120 s.

Conversely, increasing the density ratio (from 0.91 to 1.02) without any layering results in minor variations of dike asymmetry (from 1.93 to 2.31 in experiments 17, 19, and 24, Figures 3c and S2a–S2c).

Layering also promotes eruption more distant from the injection point (X ranging from 5.7 to 9 cm in experiments 24 and 23 respectively and from 0 to 3.1 cm in experiments 19 and 21, respectively, Figure 3c). The longest distance was observed for $E_u/E_l = 1.32$ which is our highest rigidity ratio in experiments with topography (experiment 23 in Figure 3d). In contrast, a density ratio increase in experiments without layering (17, 19, and 24) does not promote a more distant eruption ($X = 4.7$, 0, and 5.7 cm, respectively; Figure 3c). Finally, an increased inflow rate (experiment 20b, $d_2/d_1 = 1.8$, Figure S2d) slightly inhibits propagation toward the plain (experiment 17, $d_2/d_1 = 2.2$, Figure 3c).

3.2. Set 2 (Injection From the Side)

In Set 2 experiments, we obtained similar results to Set 1, except for the effect of the inflow rate, that in Set 2, if combined with topography, promotes lateral propagation (Figures 4a–4d).

In particular, similarly to Set 1, we observed the following:

1. A rigid upper layer promotes lateral propagation, since the increasing rigidity ratio (from 0.94 to 1.83, Figure 5a), leads to significantly longer dikes (S varies from 8.4 to 53.3 cm).
2. Density ratio variations, with constant $E_u/E_l = 0.94$, are less effective on lateral propagation, leading to similar values of dike length S and eruption distance X in experiments 33, 33b, and 52 (S = 8.5, 8.4, and 9.3 cm and X = 4.2, 4.3, and 4.6 cm respectively, Figures 5b and 5d).
3. The increase inflow rate does not affect significantly dike propagation (compare experiments 51 and 52 with 51b and 52b in Figures 5a and 5b), being the difference between the maximum and minimum values of S (henceforth called ΔS) 0.4 and 0.7 cm, for experiments 52-52b and 51-51b, respectively, and X very similar (see Table 2 and Figure 5d).

The imposed topography leads to dike lengthening and a farther eruption (implying that lateral propagation is promoted), as both S and X increase from 11.7 and 5.9 cm (in experiment 27 with no layering and flat topography) to 16.6 and 9.5 cm respectively in experiment 30 (no layering with topography, Figures 5b and 5d). The combined effect of topography with flow rate and density ratio leads also to dike lengthening: with an increased flow rate and density ratio the dike length increases from 9 (experiment 29; $Q = 0.079$ ml/s, $\rho_U/\rho_f = 0.9119$) to 12.4 cm (experiment 39; $Q = 0.435$ ml/s, $\rho_U/\rho_f = 0.9119$; Figures 6b and S5a) and 16.6 cm (experiment 30; $\rho_U/\rho_f = 1$, Figures 5b and 4b and 4c and Table 2).

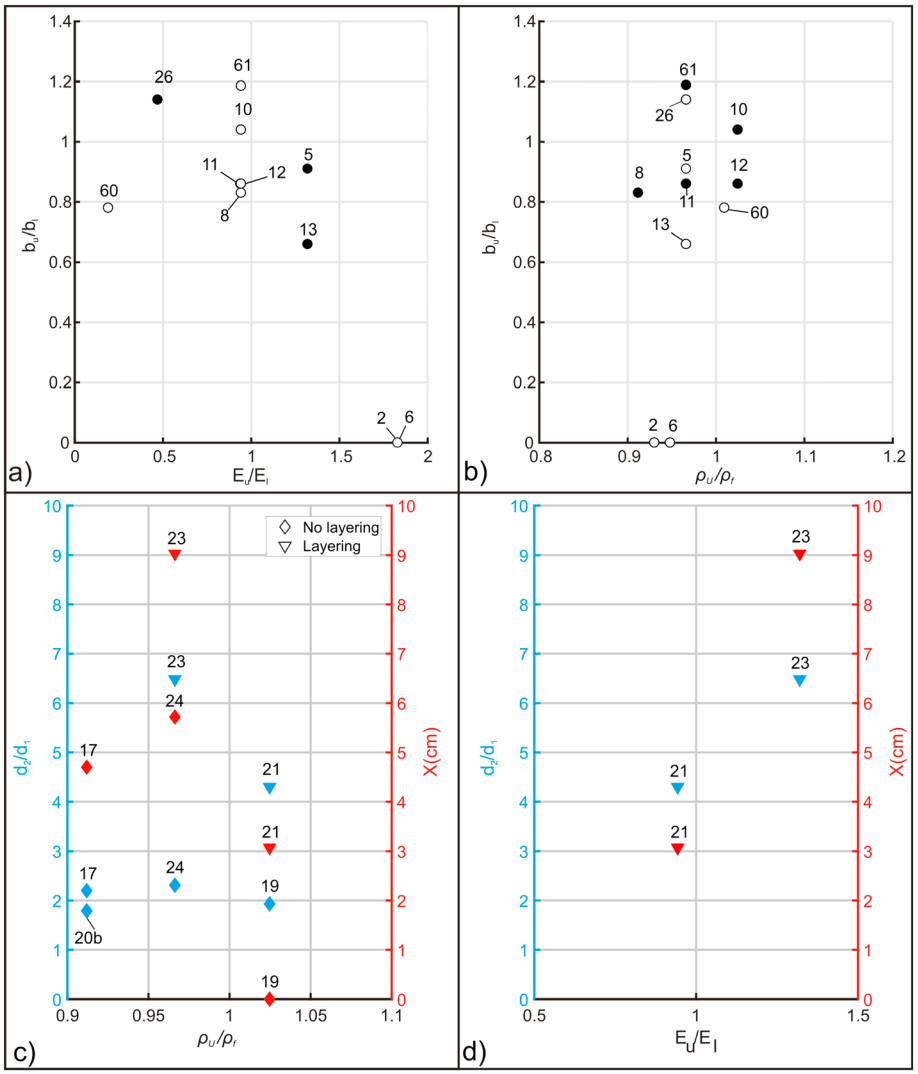

Figure 3. (a) Shape ratio (b_u/b_l) against rigidity ratio (E_u/E_l). (b) b_u/b_l against density ratio (ρ_U/ρ_f). Black circles in (a) and (b) indicate experiments in which the only changing parameter is E_u/E_l or ρ_U/ρ_f, respectively (except for experiments 12 and 13, where also the flow rate changes); the white circles indicate the experiments in which both E_u/E_l and ρ_U/ρ_f change. (c) Density ratio (ρ_U/ρ_f) against dike "asymmetry" (d_2/d_1, blue) and X (red). In X versus ρ_U/ρ_f experiment 20b is not shown because the dike did not erupt. The blue and red diamonds in (c) indicate the experiments in which the only varying parameter is ρ_U/ρ_f (except experiment 20b, in which also the flow rate changes). (d) E_u/E_l against d_2/d_1 (blue) and X (red). The numbers above each point indicate the experiment number.

Decreasing the thickness ratio (T_u/T_l) between the two layers decreases the dike length (S equal to 28.7 and 33.8 cm in experiments 36 and 32, respectively, Figures 5a and 5b), because the interface is shallower and the dike erupts earlier after crossing it.

With vertical injection (Set 1) and topography, despite being ineffective on dike asymmetry (Figure 3c), the decreasing density ratio (with no layering) promotes lateral propagation toward the plain (W = −4.6, 5.2, and −2.6 cm in experiments 17, 19, and 24 respectively; Figure 5c).

3.3. Velocity Variations

Both the horizontal (v_h) and vertical (v_v) velocities decrease with time (except for experiments 26 and 60), as a constant flux is injected into a crack with an increasing area (Figures 6a and 6b). In experiment 26 v_h increases in the first 30 s, while in experiment 60 v_v increases abruptly when the dike reaches the interface with the softer upper layer.

The v_v averaged in 30-s-long intervals ($<v_v>$) ranges from 0.17 (experiment 32) to 0.67 mm/s (experiment 33b), while the averaged v_h ($<v_h>$) ranges from 0.17 (experiment 11) to 0.60 mm/s (experiment 60); thus smaller dikes (i.e., with less surface) propagate faster vertically (Table S2).

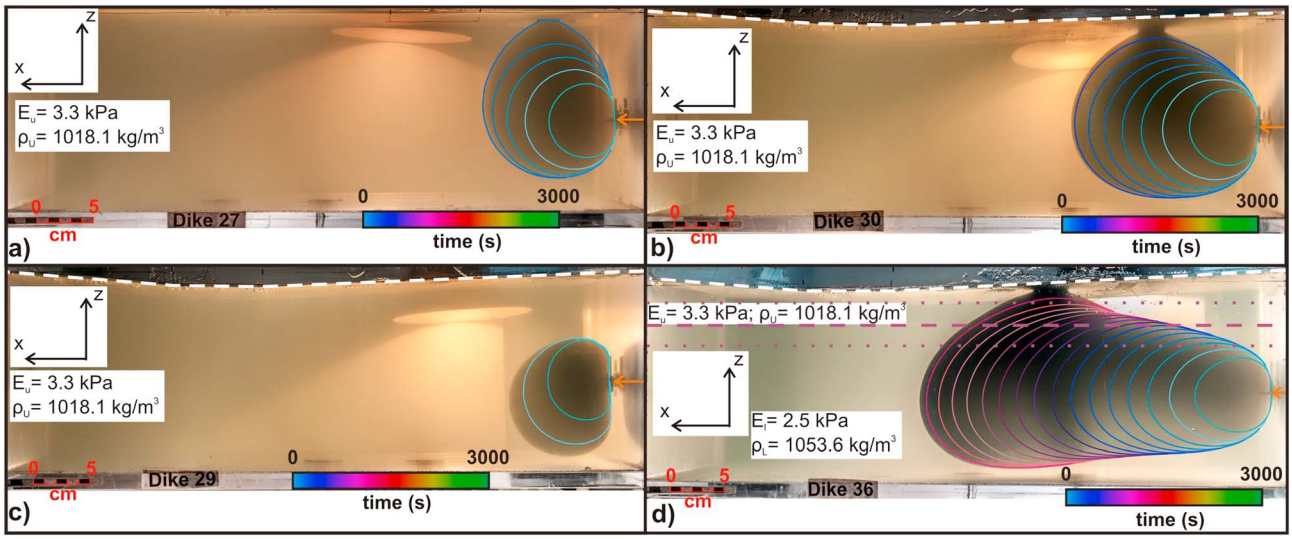

Figure 4. Section view set 2 experiments showing homogeneous gelatin without (a, experiment 27) and with topography (b, experiment 30). (c) Experiment 29 showing topography and negative buoyancy (i.e., density ratio < 1). Experiment 36 showing topography and rigidity layering. The dashed white lines indicate the topography profile. The dashed and dotted purple lines in (d) indicate the center and limits of the interface, respectively. The orange arrows indicate the injection points. The colored lines indicate the dike edge contour every 120 s.

Vertically propagating dikes ($B/H < 1$) develop with rigidity layering with $E_u/E_l < 1$ (experiments 26 and 60, Figure 7) and any simulated density layering (experiments 11, 21, 33, 33b, and 34), regardless of the injection point position and any topography.

Lateral propagating dikes ($B/H > 1$) occur with rigidity layering with $E_u/E_l > 1$ (experiments 5, 6, 23, 32, and 51, except for experiment 24 without layering), regardless of any topography and vertical or lateral injection (Figure 7).

Concentrically expanding dikes (mean $B/H \sim 1$, i.e., comprised between 0.9 and 1.1) occur with density layering and antibuoyancy (experiment 8) and homogeneous gelatin (i.e., no layering), both with (experiments 19 and 30) and without topography (experiments 27 and 57).

Vertical dikes show a stage of favored vertical propagation (B/H decrease), followed by a stage in which lateral propagation is promoted (B/H increase, except experiment 19). In particular, the smaller dikes (i.e., with less surface, experiments 33, 33b, and 34) show that lateral propagation becomes dominant after dike penetration in the upper layer (90–150 s), and not upon the dike arrival at the density interface (approximately 40 s).

V_h shows higher variations than v_v because the lateral velocity is more sensitive to the studied factors (i.e., gelatin layering and topography both promoting lateral propagation, Figures 6a and 6b). As an example, experiments 11 (only density layering) and 6 (rigidity layering), which represent two end members of vertical and lateral propagation respectively, show highly different v_h (0.30 mm/s in experiment 6 compared to 0.17 mm/s in experiment 11) despite a lower difference of v_v (0.22 mm/s in experiment 6 and 0.26 mm/s in experiment 11). This happens because in experiment 6 the dike propagates only in the lower layer (spreading laterally at the interface), being shorter than in experiment 11 (which reaches the surface) so v_v in experiment 6 is only apparently close to that of experiment 11.

In experiments 11 and 21, B/H first decreases both in the lower and upper layer and then increases. This is due to different causes: in experiment 21 the B/H increase (at $t = 400$ s) is due to the dike deflection caused by topography, whereas in experiment 11 (at $t = 900$ s) it is probably due to the effect of the free surface (Rivalta & Dahm, 2006). Moreover, the passage from the decrease to the increase of B/H in experiments 11 and 21 is less abrupt than experiments 33, 33b, and 34.

Laterally propagating dikes tend to first elongate (increase of the aspect ratio) and then to expand vertically before erupting (except for experiments 6 and 24). Experiments 23, 32, and 51 follow this trend, due to the rigidity layering (with $E_u/E_l > 1$). Otherwise, in experiment 5 the B/H increases in two different stages: (1)

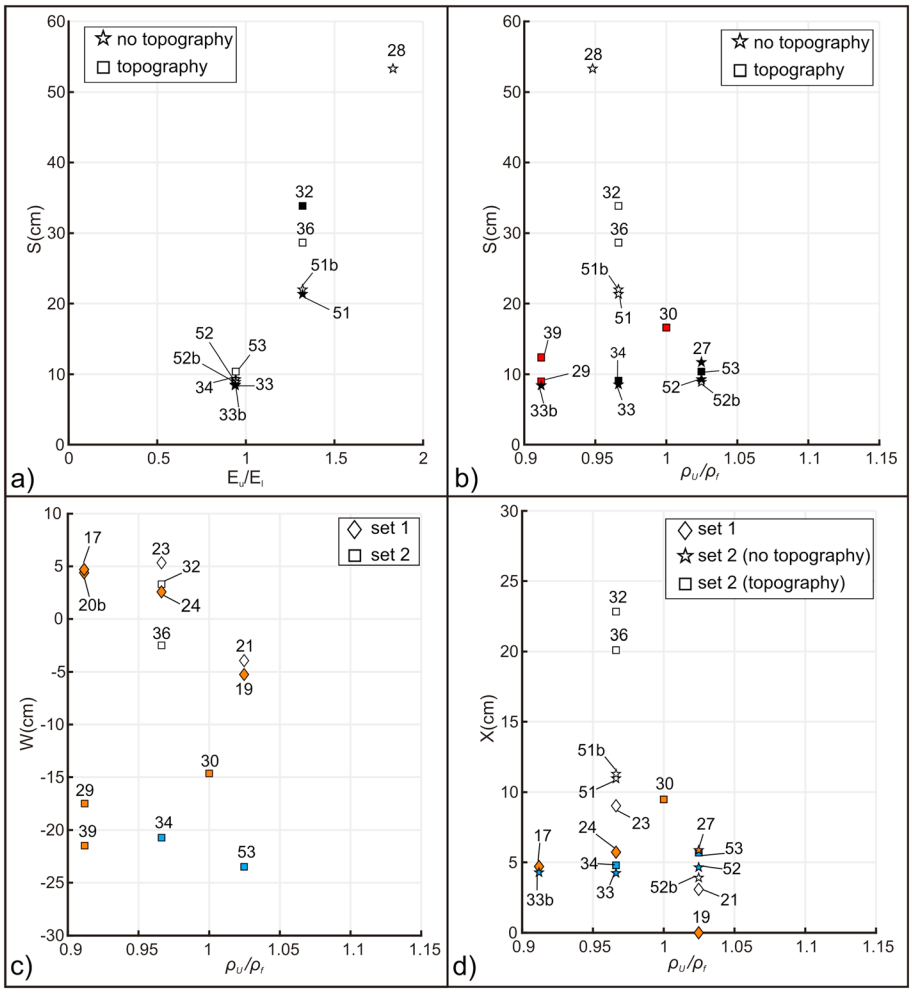

Figure 5. (a) Dike length S against E_u/E_l. (b) S against ρ_U/ρ_f. The squares and the stars indicate experiments with and without topography, respectively. Experiments 29, 30, and 39 are excluded in (a), as without layering. Numbers refer to experiments. The black and red symbols in (a) and (b) indicate the experiments in which the only changing parameter is E_u/E_l or ρ_U/ρ_f, respectively. The red symbols in (b) indicate also the experiments with homogeneous gelatin (no layering). (c) W against ρ_U/ρ_f of Set 1 (diamonds) and Set 2 experiments (squares). The positive values of W indicate that the dike tip passed below the plain edge. Experiments 28, 33, and 33b are excluded, as without topography. (d) X against ρ_U/ρ_f of Set 1 (diamonds) and Set 2 experiments (with and without topography, stars and squares, respectively). Experiments 20b, 28, 29, and 39 are excluded because the dike did not erupt. In both (c) and (d) the blue and orange symbols indicate the experiments whose only changing parameter is ρ_U/ρ_f. The orange symbols indicate also the experiments with homogeneous gelatin (no layering).

initial water injection in the lower layer and (2) dike arrival at the interface (350 s, rigidity layering). However, in both the lower and the upper layers the dike shows a similar (and constant) aspect ratio rate increase.

Experiments 6 and 24 show two stages of favored vertical and lateral propagation, similarly to the vertical propagating dikes. In particular, experiment 24 isolates the effect of topography (favoring lateral propagation) on dike kinematics: B/H increases after an initial stage of favored vertical propagation but, because there is no layering, the aspect ratio increase is due only to the effect of topography (which promotes downslope propagation of the dike). In experiment 6, the high B/H decrease is due to the positive buoyancy in the lower layer that favors vertical propagation. The abrupt switch to the high B/H increase (t = 90 s) is due to dike approaching the interface with $E_u/E_l = 1.83$.

In experiments with $E_u/E_l < 1$ the interface with the softer layer leads to a vertical acceleration of the dike. In particular, experiments 26 and 60 show a different trend: in experiment 26 ($E_u/E_l = 0.47$), the aspect ratio is almost constant with time (except for an abrupt increase in the first 60 s), showing a slight decrease as the dike approaches the interface (from 60 to 400 s) and a slight increase as the dike within the upper layer approaches the surface (from 400 to 630 s). In experiment 60 (E_u/E_l = 0.19) the aspect ratio is nearly

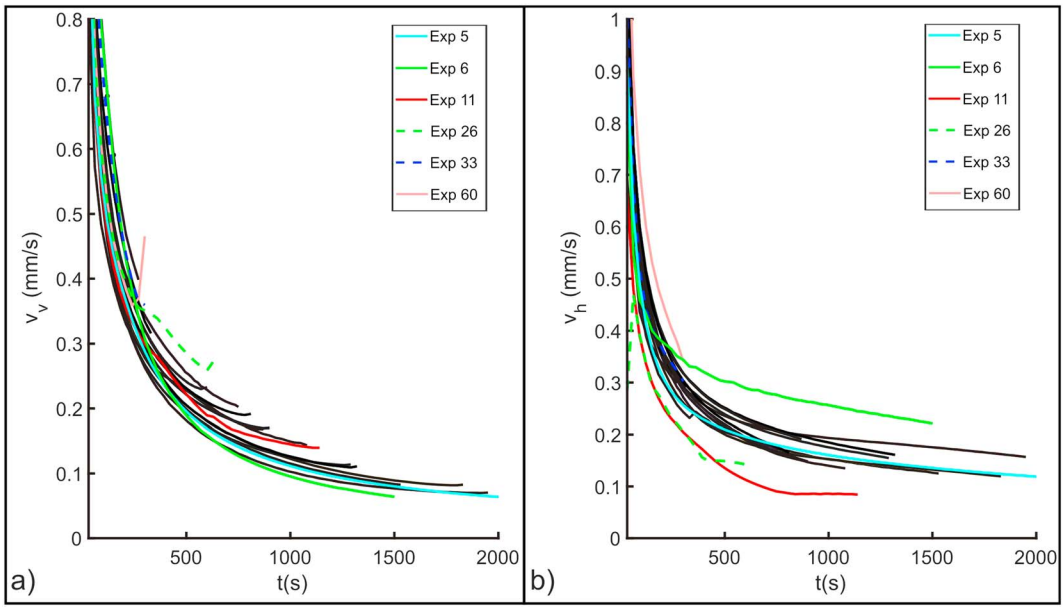

Figure 6. (a) Vertical dike velocity (v_v) against time. (b) Horizontal dike velocity (v_h) against time. Only the most representative experiments (5, 6, 11, 26, 33, and 60) are highlighted in color; otherwise, they are in black.

constant as the dike propagated in the lower layer (until 240 s), then it accelerates vertically (*B*/*H* decrease) penetrating the interface with the softer upper layer.

4. Discussion

4.1. Interpretation of the Experiments

Our results for both sets show that lateral dike propagation is promoted most efficiently with rigidity layering than with density layering and density ratio. This is supported, in Set 1, by the dikes propagating more in the lower layer when increasing the rigidity ratio. With density layering and density ratio changes, the shape variability is quite small (limited to about $\Delta b_u/b_l = 0.2$); thus, all dikes are vertical. Analogously, dikes in Set 2 with higher rigidity ratio are longer (up to 53.3 cm), whereas length variations are small with density layering (ΔS ranging from 0.9 to 1.3 cm, Figures 5a and 5b).

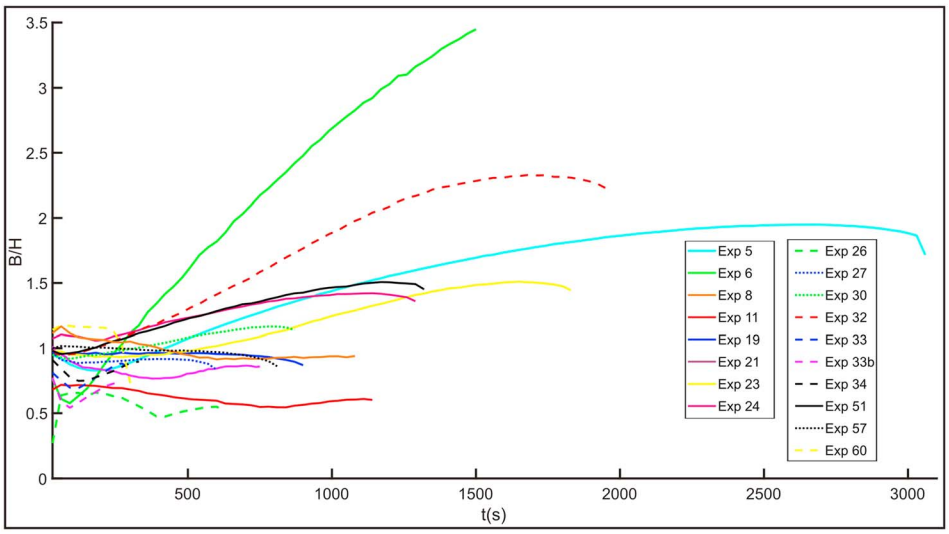

Figure 7. Dike aspect ratio (*B*/*H*) against time.

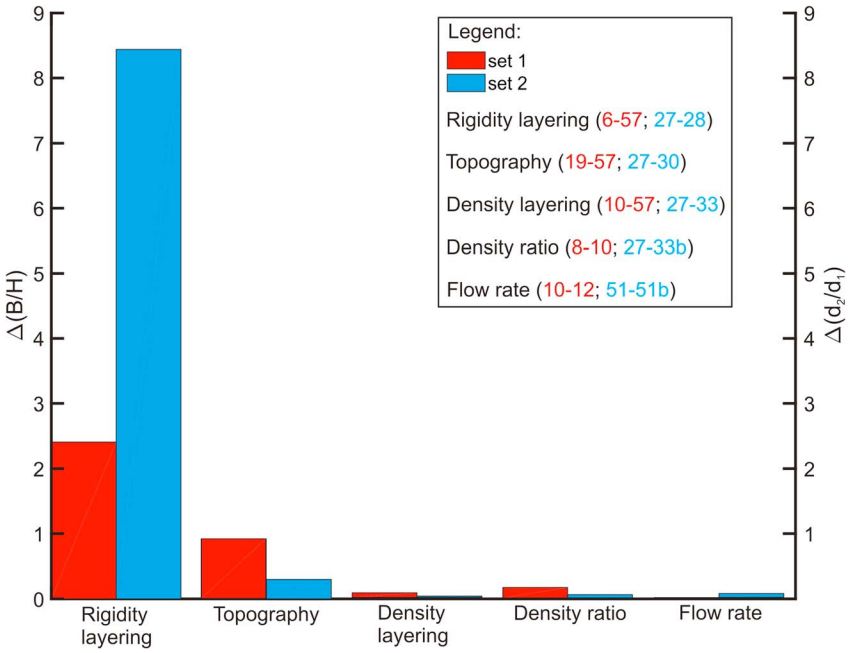

Figure 8. Histogram showing the aspect ratio difference $\Delta(B/H)$, left *y* axis, for the selected pairs of experiments (indicated in the legend). The column of Set 1 and topography refers to the variation of the dike asymmetry (Δ (d_2/d_1), right *y* axis) of experiments 19 and 57.

Concerning topography, in both sets all the dikes were elongated toward the plain, highlighting lateral propagation. This is due to the stress component normal to the dike plane (i.e., σ_2; Urbani et al., 2017) that decreases downslope, squeezing the dike toward the plain, and increases upslope, hindering further dike propagation.

To understand the different behavior of the inflow rate combined with topography between Set 1 and Set 2, we must examine the effects of the position of the injection point. In fact, negative buoyancy (experiments 17, 20b, 29, and 39) drives the dike downward, but only in Set 2 (experiments 29 and 39) the dike is free to descend, whereas in Set 1 (experiments 17 and 20b) the floor of the box prevents negatively buoyant dikes propagating downward. Therefore, the difference might be due to a boundary effect caused by the box.

Dike kinematics suggests that rigidity layering favors lateral dike velocity (and thus propagation), highlighting the subordinate role of density layering ($B/H > 1$ in experiments 5, 6, 23, 32, and 51 and $B/H < 1$ in experiments 11, 21, 33, 33b, and 34; Figure 7), similarly to what observed in the geometrical analysis.

The role of density ratio on dike propagation is less straightforward, as experiments 19 and 24 (which differ only in density ratio; Table 1 and Figure 3c) show a different evolution of the aspect ratio (Figure 7), despite their comparable final shape (see d_2/d_1 values in Figure 3c and Table 1). In experiment 19, $B/H \sim 1$ and approximately constant, whereas in experiment 24 B/H increases after an initial decrease, reaching 1 (Figure 7 and Table 1). Therefore, density ratio variations influence more the dike kinematics (i.e., the dike shape evolution) than their geometry (i.e., the dike final shape).

The kinematic analysis shows that no dike propagated with a steady state regime, as in a homogenous medium (Menand & Tait, 2002; Takada, 1990). The exception of experiment 19 (approximately constant B/H throughout the entire experiment) is probably related to the following: (1) the combined effect of the topography profile and density ratio, which is almost 1 ($\rho_U/\rho_f = 1.0247$), that did not influence dike kinematics and (2) the propagation of a crack with constant and finite volume (Menand & Tait, 2002; Takada, 1990) conversely to our continuously fed crack (thus increasing its volume).

4.2. Hierarchy of Parameters Controlling Lateral and Vertical Propagation

Our results suggest a hierarchy between the investigated factors (rigidity and density layering, density ratio, flow rate, and topography) based on the variations of the aspect ratio, $\Delta(B/H)$, of selected pairs of experimental dikes (Figure 8) with only one changing parameter (among E_u/E_l, ρ_U/ρ_f, Q, and topography) per time. In

particular, we compare experiment 57 (without layering and with flat topography) with experiment 6, since the latter shows the maximum B/H in experiments with $E_u/E_l > 1$; we then compare experiments 8 and 10 with 27 and 33b, since both pairs show the highest density ratio variation (equal to 0.11).

Only in the case of Set 1 with topography the indicated value is calculated from the dike asymmetry variation, $\Delta(d_2/d_1)$ (right y axis in Figure 8), rather than from the aspect ratio B/H.

Considering this, the hierarchy is defined as follows:

Set 1 (Vertical injection)

1. Rigidity layering; $\Delta(B/H) = 2.41$ (experiments 6 and 57).
2. Topography; $\Delta(d_2/d_1) = 0.94$ (experiments 19 and 57).
3. Density ratio; $\Delta(B/H) = 0.16$ (experiments 8 and 10).
4. Density layering; $\Delta(B/H) = 0.07$ (experiments 10 and 57).
5. Flow rate; $\Delta(B/H) = 0$ (experiments 10 and 12).

Set 2 (Lateral injection)

1. Rigidity layering; $\Delta(B/H) = 8.44$ (experiments 27 and 28).
2. Topography; $\Delta(B/H) = 0.30$ (experiments 27 and 30).
3. Flow rate; $\Delta(B/H) = 0.06$ (experiments 51 and 51b).
4. Density ratio; $\Delta(B/H) = 0.05$ (experiments 27 and 33b).
5. Density layering; $\Delta(B/H) = 0.02$ (experiments 27 and 33).

This hierarchy shows that rigidity layering and topography predominate in promoting lateral propagation, regardless of any position of the injection (Set 1 or Set 2). This implies that a stiffer layer overlying a softer layer favors lateral dike propagation (or its vertical arrest) more efficiently than the LNB, which has been previously proposed by analytical (Lister, 1990, 1991; Lister & Kerr, 1991; Rubin, 1995; Ryan, 1994, and references therein) and numerical models (Taisne & Jaupart, 2009) as the factor driving laterally propagating dikes.

Lateral dikes have never been observed with a neutral buoyancy interface in previous analogue models, using both air (thus with a buoyancy 1 order of magnitude higher than here; Rivalta et al., 2005) or water (Kavanagh et al., 2006; Ritter et al., 2013) as magma analogue. This provides additional support to the importance of rigidity layering in driving lateral dike propagation. Also, in our experiments we never witnessed lateral propagation at the LNB, thus confirming previous results.

An exception to this is Lister and Kerr (1991): they obtained lateral dike propagation at the LNB injecting glycerol in agar. The host medium showed a density gradient spanning from 1,066 to 1,310 kg/m, while glycerol density was 1,221 kg/m with the LNB at 18.1 cm from the surface. The discrepancies with our models may be explained by the higher antibuoyancy (i.e., a less buoyant fluid) and thickness of the low-density layer, -155 kg/m (within the natural range of -300 + 300 kg/m^3) and 18.1 cm, respectively, compared to -35 kg/m^3 and 15.5 cm (experiment 61, Table 1). This implies a deeper equilibrium position of their experimental dikes (at which they start to propagate laterally), allowing a more significant lateral propagation before the eruption with respect to our dikes.

The discrepancies between our experiments and the analytical and numerical models on the role of LNB may be explained by the finite thickness of the layers in our experiments. Indeed, both analytical and numerical models assume an infinite thickness of the regions above and below the interface stating that the dikes, before propagating laterally at the interface, should penetrate the low-density layers over a certain length threshold before reaching the equilibrium (Lister, 1990; Maccaferri et al., 2011; Taisne & Jaupart, 2009; Townsend et al., 2017). Therefore, the thickness of the upper layer in our experiments may have been below this threshold, so that the dikes erupted before showing a consistent lateral propagation, which may have been expected with a thicker upper layer. This is supported by the increasing dike aspect ratio in experiment 61 (with T_u = 15.5 cm and $B/H = 1$) with respect to experiment 11 (with T_u = 7.3 cm and $B/H = 0.70$), both showing the same density contrasts between the gelatin and the injected fluid. In experiment 61 (thicker low-density layer) the dike showed a more consistent lateral propagation at the LNB, probably because it reached a stable height in the upper layer before reaching the surface. Since the stable height increases with decreasing density contrasts between host rock and magma ($\Delta\rho$) (Townsend et al., 2017), and the negative density contrasts are relatively small (up to -98 kg/m^3), probably the dikes in density layering experiments

erupted before reaching the vertical equilibrium. However, since with comparable layer thicknesses the B/H variation with rigidity layering is still much higher, this does not affect the proposed hierarchy, confirming the effectiveness of rigidity layering with respect to density layering and density ratio variations.

Moreover, most analytical and numerical models are formulated in two dimensions, focusing either on what controls the propagation of the dike tip in a specific direction (Rivalta et al., 2015) or on the conditions that determine the dike's vertical equilibrium position (Townsend et al., 2017). In order to compare the analogue models (such as those presented here) with the analytical and numerical ones, full 3-D models are required.

The importance of topographic loads in controlling dike propagation has been already suggested by analogue (Acocella & Tibaldi, 2005; Urbani et al., 2017) and numerical models (Corbi et al., 2015; Heimisson et al., 2015; Maccaferri et al., 2014).

In addition to previous studies, our models show that a stress gradient perpendicular to the dike plane drives lateral propagation, especially if assisted by a stiff upper layer that prevents dike ascent. The dike tail is compressed and the dike front squeezed toward the plain, until the normal stress start to increase upslope, compressing the dike tip. This explains both the asymmetry and the increased length in both Set 1 and Set 2 experiments, respectively, plus the arrest below the plain of all of the experimental dikes, as already noticed only for Set 2 experiments by Urbani et al. (2017).

Compared to rigidity layering and topography, it is challenging to define hierarchies among density ratio, density layering, and flow rate because Δ (B/H) shows a low variability (ranging from 0 to 0.16).

4.3. Comparison to Nature

The studied range of density contrasts is small compared to the ranges occurring in nature. Indeed, considering that the density of silicate melts ranges from 2,200 to 2,800 kg/m^3 (Bottinga & Weill, 1970; Murase & McBirney, 1973) and the density of crustal rocks ranges from 1,600 to 3,100 kg/m^3 (Turcotte & Schubert, 2014), we obtain that $\Delta\rho$ spans from $-1{,}200$ to 900 kg/m^3. Excluding extreme values, typical density contrast in recent diking events span from -300 to +300 kg/m^3 as for El Hierro 2011–2012 (Figure S9a; Martí et al., 2013, 2017; Fullea et al., 2015), Bardarbunga 2014–2015 (Figure S9b; M. T. Gudmundsson & Hognadottir, 2007; Haddadi et al., 2015; Hudson et al., 2017), and Kilauea (Ryan, 1987; Zucca et al., 1982). In case of such negative density contrasts (i.e., a less buoyant magma) the dike stable height is relatively low (1–2 km; Townsend et al., 2017), suggesting that the dikes were vertically trapped at high depths and propagated laterally for tens of kilometers before erupting. The negative density contrasts in our models are a subset of natural ones (up to -98 kg/m^3), implying a higher stable height (thus a shallower equilibrium position). The maximum stable height (H_m) for our models can be calculated from (e.g. Rivalta et al., 2015):

$$H_m = 2\left(K_c/\Delta\rho g\sqrt{\pi}\right)^{2/3} \tag{4}$$

Therefore, assuming $K_c = 10^{-4}$ MPa m$^{1/2}$ and $\Delta\rho g = -0.4 \times 10^{-3}$ MPa/m (from $\Delta\rho = -35$ kg/m^3, experiment 61), H_m (models) = 54 cm.

This means that in all our density layering experiments the dikes reached the equilibrium height after the eruption (see values of T_u in Table 1), preventing a significant lateral propagation, also because we have not considered any extensional stress which may have assisted antibuoyancy to stop dike ascent.

However, also the rigidity contrasts tested in the experiments represent only a small portion of the natural cases. Indeed, we tested a rigidity ratio E_u/E_l ranging from 0.1 to ~2, whereas in nature it spans from 0.09 to 11 (Turcotte & Schubert, 2014), thus up to 1 order of magnitude higher with respect to our models. Therefore, also the tested effect of rigidity layering represents a conservative estimate of its influence on lateral dike propagation occurring in nature, thus still supporting the highest efficiency of rigidity layering in this study. Nevertheless, as the fracture toughness (not tested in our experiments) in natural rocks should vary by orders of magnitude (10^6–10^9 Pa m$^{1/2}$), it may be even more important than rigidity.

In nature, the rigidity decrease with depth, leading to rigidity inversions (i.e., stiff layer above a weak one, as we modeled here), may be due to soft scoria layers capped by stiff lava flows, as in Afar (Abbate et al., 2015) and Iceland (A. Gudmundsson, 2005). Moreover, at a broader scale, partial melt or superheated steam in geothermal areas decreases the rigidity of the host rock by thermal weakening (Heap et al., 2013), so that

it becomes more compliant at high depths, as geophysically detected at Askja and Krafla (Iceland; Mitchell et al., 2013; Schuler et al., 2015), Kilauea's East Rift Zone (Hawaii; Haslinger et al., 2001), Afar (Desissa et al., 2013), and Canary Islands (Martí et al., 2017). Therefore, these wide scale rigidity inversions due to thermal and/or chemical alteration of the host rock seem common in volcanic areas and rift zones and should encourage a dike to propagate laterally at the interface with the stiffer zone, as for example also locally observed during the 2004 Asama (Japan) and 2011–2012 El Hierro (Canary Islands) eruptions (Aoki et al., 2009; Martí et al., 2013).

Recent natural diking events such as Bardarbunga 2014–2015 (Sigmundsson et al., 2015) and Dabbahu 2005–2010 (Belachew et al., 2011; Ebinger et al., 2010) highlighted the relevant role of topography (Urbani et al., 2017) in controlling dike propagation. Indeed, both these episodes show that the dike stopped before a high relief, as observed in our models. Some of our experiments, with rigidity layering (experiments 23 and 32, Table 1) or strong negative buoyancy (experiment 17), showed that the dike tip propagated below the plain as during the Bardarbunga eruption (Sigmundsson et al., 2015), but, contrary to Bardarbunga, erupting before the plain. However, during the eruption, three "ice cauldrons" were observed on the Vatnajökull ice cap (Reynolds et al., 2017), suggesting that minor subglacial eruptions had occurred also before the main eruption inside the plain. During the Dabbahu diking episode the northern section of the dike propagated upslope erupting on NE flank of the volcanic edifice, in contrast with our experiments, which suggest that upslope propagation is inhibited. In this case, the effect on crustal stresses of a lateral thermal gradient of the crust may have overcome the effect of topography (Grandin et al., 2012), favoring upslope dike propagation.

5. Conclusions

Our experimental results suggest the following:

1. Rigidity layering (i.e., stiff layers overlying soft layers) and topography (i.e., a slope perpendicular to the dike plane) are the most important factors that promote lateral dike propagation, especially if combined together. The joint effect of rigidity layering and topography should be considered to explain the lateral propagation observed in recent diking events.
2. Density ratio between magma and host rock, density layering, and flow rate show a lower influence on dike propagation. In particular, we did not observe any lateral propagation at the LNB, despite what proposed by previous analytical and numerical models.

The proposed hierarchy should be completed adding the processes that influence dike propagation not considered in this study such as regional tectonics, magma solidification, volatile exsolution, and preexisting fractures in the host rock.

Acknowledgments
Giulia Sili provided technical support during the experiments. Matteo Trolese provided useful suggestions for the image processing. Malte C. Ritter shared his data on gelatin rigidity. Janine Kavanagh provided helpful advices for the setting of the analogue models. Benoit Taisne and Nicolas Le Corvec kindly reviewed an earlier version of the manuscript, providing helpful suggestions. Daniele Trippanera and Kirsten Elger helped for the data storage in the Multi-Scale Laboratories database. This work was financed by the Italian government (MIUR) grants to Roma Tre PhD School in Earth Sciences. Any user can access the data of this work at http://doi.org/10.5880/fidgeo.2018.012 (Urbani et al., 2018) through the Multi-Scale Laboratories database in the framework of the European Observing System project (EPOS). Two anonymous reviewers are acknowledged for their constructive reviews.

References

Abbate, E., Bruni, P., & Sagri, M. (2015). Geology of Ethiopia: A review and geomorphological perspectives. In P. Billi (Ed.), *Landscapes and landforms of Ethiopia, world geomorphological landscapes* (pp. 33–64). Dordrecht, Netherlands: Springer Science + Business Media. https://doi.org/10.1007/978-94-017-8026-1_2

Acocella, V., & Neri, M. (2003). What makes flank eruptions? The 2001 Etna eruption and its possible triggering mechanisms. *Bulletin of Volcanology*, *65*(7), 517–529. https://doi.org/10.1007/s00445-003-0280-3

Acocella, V., & Neri, M. (2009). Dike propagation in volcanic edifices: Overview and possible developments. *Tectonophysics*, *471*(1-2), 67–77. https://doi.org/10.1016/j.tecto.2008.10.002

Acocella, V., Porreca, M., Neri, M., Massimi, E., & Mattei, M. (2006). Propagation of dikes at Vesuvio (Italy) and the effect of Mt. Somma. *Geophysical Research Letters*, *33*, L08301. https://doi.org/10.1029/2005GL025590

Acocella, V., & Tibaldi, A. (2005). Dike propagation driven by volcano collapse: A general model tested at Stromboli, Italy. *Geophysical Research Letters*, *32*, L08308. https://doi.org/10.1029/2004GL022248

Aoki, Y., Takeo, M., Aoyama, H., Fujimatsu, J., Matsumoto, S., Miyamachi, H., et al. (2009). *P*-wave velocity structure beneath Asama Volcano, Japan, inferred from active source seismic experiment. *Journal of Volcanology and Geothermal Research*, *187*(3-4), 272–277. https://doi.org/10.1016/j.jvolgeores.2009.09.004

Ayele, A., Keir, D., Ebinger, C., Wright, T. J., Stuart, G. W., Buck, W. R., et al. (2009). September 2005 mega-dike emplacement in the Manda-Harraro nascent oceanic rift (Afar depression). *Geophysical Research Letters*, *36*, L20306. https://doi.org/10.1029/2009GL039605

Bagnardi, M., Amelung, F., & Poland, M. P. (2013). A new model for the growth of basaltic shields based on deformation of Fernandina volcano, Galápagos Islands. *Earth and Planetary Science Letters*, *377-378*, 358–366. https://doi.org/10.1016/j.epsl.2013.07.016

Battaglia, J., Ferrazzini, V., Staudacher, T., Aki, K., & Cheminèe, J. L. (2005). Pre-eruptive migration of earthquakes at the Piton de la Fournaise volcano (Rèunion Island). *Geophysical Journal International*, *161*(2), 549–558. https://doi.org/10.1111/j.1365-246X.2005.02606.x

Belachew, M., Ebinger, C., Coté, D., Keir, D., Rowland, J. V., Hammond, J. O. S., & Ayele, A. (2011). Comparison of dike intrusions in an incipient seafloor-spreading segment in Afar, Ethiopia: Seismicity perspectives. *Journal of Geophysical Research*, *116*, B06405. https://doi.org/10.1029/2010JB007908

Biggs, J., Amelung, F., Gourmelen, N., Dixon, T. H., & Kim, S. (2009). InSAR observations of 2007 Tanzania rifting episode reveal mixed fault and dyke extension in an immature continental rift. *Geophysical Journal International*, *179*(1), 549–558. https://doi.org/10.1111/j.1365-246X.2009.04262.x

Bottinga, Y., & Weill, D. F. (1970). Densities of liquid silicate systems calculated from partial molar volumes of oxide components. *American Journal of Science*, *269*(2), 169–182. https://doi.org/10.2475/ajs.269.2.169

Brizzi, S., Funiciello, F., Corbi, F., Di Giuseppe, E., & Mojoli, G. (2016). Salt matters: How salt affects the rheological and physical properties of gelatine for analogue modelling. *Tectonophysics*, *679*, 88–101. https://doi.org/10.1016/j.tecto.2016.04.021

Buck, W. R., Einarsson, P., & Brandsdóttir, B. (2006). Tectonic stress and magma chamber size as controls on dike propagation: Constraints from the 1975–1984 Krafla rifting episode. *Journal of Geophysical Research*, *111*, B12404. https://doi.org/10.1029/2005JB003879

Chadwick, W. W., & Dieterich, J. H. (1995). Mechanical modeling of circumferential and radial dike intrusion on Galapagos volcanoes. *Journal of Volcanology and Geothermal Research*, *66*(1-4), 37–52. https://doi.org/10.1016/0377-0273(94)00060-T

Chanceaux, L., & Menand, T. (2014). Solidification effects on sill formation: An experimental approach. *Earth and Planetary Science Letters*, *403*, 79–88. https://doi.org/10.1016/j.epsl.2014.06.018

Chanceaux, L., & Menand, T. (2016). The effects of solidification on sill propagation dynamics and morphology. *Earth and Planetary Science Letters*, *442*, 39–50. https://doi.org/10.1016/j.epsl.2016.02.044

Corbi, F., Rivalta, E., Pinel, V., Maccaferri, F., & Acocella, V. (2016). Understanding the link between circumferential dikes and eruptive fissures around calderas based on numerical and analog models. *Geophysical Research Letters*, *43*, 6212–6219. https://doi.org/10.1002/2016GL068721

Corbi, F., Rivalta, E., Pinel, V., Maccaferri, F., Bagnardi, M., & Acocella, V. (2015). How caldera collapse shapes the shallow emplacement and transfer of magma in active volcanoes. *Earth and Planetary Science Letters*, *431*, 287–293. https://doi.org/10.1016/j.epsl.2015.09.028

Dahm, T. (2000). Numerical simulations of the propagation path and arrest of fluid-filled fractures in the earth. *Geophysical Journal International*, *141*, 623–638. https://doi.org/10.1046/j.1365-246x.2000.00102.x

Daniels, K. A., & Menand, T. (2015). An experimental investigation of dyke injection under regional extensional stress. *Journal of Geophysical Research: Solid Earth*, *120*(3), 2014–2035. https://doi.org/10.1002/2014JB011627

Desissa, M., Johnson, N. E., Whaler, K. A., Hautot, S., Fisseha, S., & Dawes, G. J. K. (2013). A mantle magma reservoir beneath an incipient mid-ocean ridge in Afar, Ethiopia. *Nature Geoscience*, *6*(10), 861–865. https://doi.org/10.1038/ngeo1925

Di Giuseppe, E., Funiciello, F., Corbi, F., Ranalli, G., & Mojoli, G. (2009). Gelatins as rock analogs: A systematic study of their rheological and physical properties. *Tectonophysics*, *473*(3–4), 391–403. https://doi.org/10.1016/j.tecto.2009.03.012

Ebinger, C. J., Ayele, A., Keir, D., Rowland, J., Yirgu, G., Wright, T., et al. (2010). Length and timescales of rift faulting and magma intrusion: The Afar rifting cycle from 2005 to present. *Annual Review of Earth and Planetary Sciences*, *38*(1), 439–466. https://doi.org/10.1146/annurev-earth-040809-152333

Einarsson, P., & Brandsdóttir, B. (1980). Seismological evidence for Lateral magma intrusion during the July 1978 deflation of the Krafla volcano in NE-Iceland. *Journal of Geophysics*, 160–165. https://doi.org/10.2172/890964

Fialko, Y. A., & Rubin, A. M. (1999). What controls the along-strike slopes of volcanic rift zones? *Journal of Geophysical Research*, *104*, 20,007–20,020. https://doi.org/10.1029/1999JB900143

Fiske, R. S., & Jackson, E. D. (1972). Orientation and growth of Hawaiian volcanic rifts: The effect of regional structure and gravitational stresses. *Proceedings of the Royal Society of London A*, *329*(1578), 299–326. https://doi.org/10.1098/rspa.1972.0115

Fukushima, Y., Cayol, V., & Durand, P. (2005). Finding realistic dike models from interferometric synthetic aperture radar data: The February 2000 eruption at Piton de la Fournaise. *Journal of Geophysical Research*, *110*, B03206. https://doi.org/10.1029/2004JB003268

Fullea, J., Camacho, A. G., Negredo, A. M., & Fernández, J. (2015). The Canary Islands hot spot: New insights from 3D coupled geophysical–petrological modelling of the lithosphere and uppermost mantle. *Earth and Planetary Science Letters*, *409*, 71–88. https://doi.org/10.1016/j.epsl.2014.10.038

Grandin, R., Socquet, A., Doubre, C., Jacques, E., & King, G. C. P. (2012). Elastic thickness control of lateral dyke intrusion at mid-ocean ridges. *Earth and Planetary Science Letters*, *319-320*, 83–95. https://doi.org/10.1016/j.epsl.2011.12.011

Gudmundsson, A. (2003). Surface stresses associated with arrested dykes in rift zones. *Bulletin of Volcanology*, *65*(8), 606–619. https://doi.org/10.1007/s00445-003-0289-7

Gudmundsson, A. (2005). Effects of mechanical layering on the development of normal faults and dykes in Iceland. *Geodinamica Acta*, *18*(1), 11–30. https://doi.org/10.3166/ga.18.11-30

Gudmundsson, A. (2006). How local stresses control magma-chamber ruptures, dyke injections, and eruptions in composite volcanoes. *Earth-Science Reviews*, *79*(1-2), 1–31. https://doi.org/10.1016/j.earscirev.2006.06.006

Gudmundsson, M. T., & Hognadottir, T. (2007). Volcanic systems and calderas in the Vatnajokull region, central Iceland: Constraints on crustal structure from gravity data. *Journal of Geodynamics*, *43*(1), 153–169. https://doi.org/10.1016/j.jog.2006.09.015

Haddadi, B., Sigmarsson, O., & Devidal, J. L. (2015). *Determining intensive parameters through clinopyroxene-liquid equilibrium in Grímsvötn 2011 and Bárðarbunga 2014 basalts*. Paper Presented at European Geoscience Union General Assembly 2015, Vienna, Austria.

Hartley, M. E., & Thordarson, T. (2012). Formation of Öskjuvatn caldera at Askja, North Iceland : Mechanism of caldera collapse and implications for the lateral flow hypothesis. *Journal of Volcanology and Geothermal Research*, *227-228*, 85–101. https://doi.org/10.1016/j.jvolgeores.2012.02.009

Hartley, M. E., & Thordarson, T. (2013). The 1874–1876 volcano-tectonic episode at Askja, North Iceland: Lateral flow revisited. *Geochemistry, Geophysics, Geosystems*, *14*, 2286–2309. https://doi.org/10.1002/ggge.20151

Haslinger, F., Thurber, C., Mandernach, M., & Okubo, P. (2001). Tomographic image of P-velocity structure beneath Kilauea's East Rift zone and south flank: Seismic evidence for a deep magma body. *Geophysical Research Letters*, *28*, 375–378. https://doi.org/10.1029/2000GL012018

Heap, M. J., Mollo, S., Vinciguerra, S., Lavallée, Y., Hess, K.-U., Dingwell, D. B., et al. (2013). Thermal weakening of the carbonate basement under Mt. Etna volcano (Italy): Implications for volcano instability. *Journal of Volcanology and Geothermal Research*, *250*, 42–60. https://doi.org/10.1016/j.jvolgeores.2012.10.004

Heimisson, E. R., Hooper, A., & Sigmundsson, F. (2015). Forecasting the path of a laterally propagating dike. *Journal of Geophysical Research: Solid Earth*, *120*, 8774–8792. https://doi.org/10.1002/2015JB012402

Hudson, T. S., White, R. S., Greenfield, T., Ágústsdóttir, T., Brisbourne, A., & Green, R. G. (2017). Deep crustal melt plumbing of Bárðarbunga volcano, Iceland. *Geophysical Research Letters*, *44*, 8785–8794. https://doi.org/10.1002/2017GL074749

Ito, G., & Martel, S. J. (2002). Focusing of magma in the upper mantle through dike interaction. *Journal of Geophysical Research*, *107*(B10), 2223. https://doi.org/10.1029/2001JB000251

Kavanagh, J. L., Menand, T., & Daniels, K. A. (2013). Gelatine as a crustal analogue: Determining elastic properties for modelling magmatic intrusions. *Tectonophysics*, *582*, 101–111. https://doi.org/10.1016/j.tecto.2012.09.032

Kavanagh, J. L., Menand, T., & Sparks, R. S. J. (2006). An experimental investigation of sill formation and propagation in layered elastic media. *Earth and Planetary Science Letters*, *245*(3-4), 799–813. https://doi.org/10.1016/j.epsl.2006.03.025

Kervyn, M., Ernst, G. G. J., De Vries, B. V. W., Mathieu, L., & Jacobs, P. (2009). Volcano load control on dyke propagation and vent distribution: Insights from analogue modeling. *Journal of Geophysical Research*, *114*, B03401. https://doi.org/10.1029/2008JB005653

Le Corvec, N., Menand, T., & Lindsay, J. (2013). Interaction of ascending magma with pre-existing crustal fractures in monogenetic basaltic volcanism: An experimental approach. *Journal of Geophysical Research: Solid Earth*, *118*, 968–984. https://doi.org/10.1002/jgrb.50142

Lister, J. R. (1990). Buoyancy-driven fluid fracture: Similarity solutions for the horizontal and vertical propagation of fluid-filled cracks. *Journal of Fluid Mechanics*, *217*(1), 213–239. https://doi.org/10.1017/S0022112090000696

Lister, J. R. (1991). Steady solutions for feeder dykes in a density-stratified lithosphere. *Earth and Planetary Science Letters*, *107*(2), 233–242. https://doi.org/10.1016/0012-821X(91)90073-Q

Lister, J. R., & Kerr, R. C. (1991). Fluid-mechanical models of crack propagation and their application to magma transport in dykes. *Journal of Geophysical Research*, *96*, 10,049–10,077. https://doi.org/10.1029/91JB00600

Maccaferri, F., Bonafede, M., & Rivalta, E. (2011). A quantitative study of the mechanisms governing dike propagation, dike arrest and sill formation. *Journal of Volcanology and Geothermal Research*, *208*(1–2), 39–50. https://doi.org/10.1016/j.jvolgeores.2011.09.001

Maccaferri, F., Rivalta, E., Keir, D., & Acocella, V. (2014). Off-rift volcanism in rift zones determined by crustal unloading. *Nature Geoscience*, *7*(4), 297–300. https://doi.org/10.1038/NGEO2110

Maccaferri, F., Rivalta, E., Passarelli, L., & Aoki, Y. (2016). On the mechanisms governing dike arrest: Insight from the 2000 Miyakejima dike injection. *Earth and Planetary Science Letters*, *434*, 64–74. https://doi.org/10.1016/j.epsl.2015.11.024

Martí, J., Pinel, V., López, C., Geyer, A., Abella, R., Tárraga, M., et al. (2013). Causes and mechanisms of the 2011–2012 El Hierro (Canary Islands) submarine eruption. *Journal of Geophysical Research: Solid Earth*, *118*(3), 823–839. https://doi.org/10.1002/jgrb.50087

Martí, J., Villaseñor, A., Geyer, A., López, C., & Tryggvason, A. (2017). Stress barriers controlling lateral migration of magma revealed by seismic tomography. *Scientific Reports*, *7*, 1–10. https://doi.org/10.1038/srep40757

Menand, T., Daniels, K. A., & Benghiat, P. (2010). Dyke propagation and sill formation in a compressive tectonic environment. *Journal of Geophysical Research*, *115*, B08201. https://doi.org/10.1029/2009JB006791

Menand, T., & Tait, S. R. (2001). A phenomenological model for precursor volcanic eruptions. *Nature*, *411*(6838), 678–680. https://doi.org/10.1038/35079552

Menand, T., & Tait, S. R. (2002). The propagation of a buoyant liquid-filled fissure from a source under constant pressure: An experimental approach. *Journal of Geophysical Research*, *107*(B11), 2306. https://doi.org/10.1029/2001JB000589

Mitchell, M. A., White, R. S., Roecker, S., & Greenfield, T. (2013). Tomographic image of melt storage beneath Askja Volcano, Iceland using local microseismicity. *Geophysical Research Letters*, *40*, 5040–5046. https://doi.org/10.1002/grl.50899

Muller, J. R., Ito, G., & Martel, S. J. (2001). Effects of volcano loading on dike propagation in an elastic half-space. *Journal of Geophysical Research*, *106*, 11,101–11,113. https://doi.org/10.1029/2000JB900461

Murase, T., & McBirney, A. R. (1973). Proprieties of some common igneous rocks and their melts at high temperatures. *Geological Society of America Bulletin*, *84*(11), 3563–3592. https://doi.org/10.1130/0016-7606(1973)84%3C3563:POSCIR%3E2.0.CO;2

Nobile, A., Pagli, C., Keir, D., Wright, T. J., Ayele, A., Ruch, J., & Acocella, V. (2012). Dike-fault interaction during the 2004 Dallol intrusion at the northern edge of the Erta Ale Ridge (Afar, Ethiopia). *Geophysical Research Letters*, *39*, L19305. https://doi.org/10.1029/2012GL053152

Pallister, J. S., McCausland, W. A., Jónsson, S., Lu, Z., Zahran, H. M., Hadidy, S. E., et al. (2010). Broad accommodation of rift-related extension recorded by dyke intrusion in Saudi Arabia. *Nature Geoscience*, *3*(10), 705–712. https://doi.org/10.1038/ngeo966

Peltier, A., Bachèlery, P., & Staudacher, T. (2009). Magma transport and storage at Piton de La Fournaise (La Réunion) between 1972 and 2007: A review of geophysical and geochemical data. *Journal of Volcanology and Geothermal Research*, *184*(1-2), 93–108. https://doi.org/10.1016/j.jvolgeores.2008.12.008

Pinel, V., Carrara, A., Maccaferri, F., Rivalta, E., & Corbi, F. (2017). A two-step model for dynamical dike propagation in two dimensions: Application to the July 2001 Etna eruption. *Journal of Geophysical Research: Solid Earth*, *122*, 1107–1125. https://doi.org/10.1002/2016JB013630

Pinel, V., & Jaupart, C. (2004). Magma storage and horizontal dyke injection beneath a volcanic edifice. *Earth and Planetary Science Letters*, *221*(1-4), 245–262. https://doi.org/10.1016/S0012-821X(04)00076-7

Reynolds, H. I., Gudmundsson, M. T., Högnadóttir, T., Magnússon, E., & Pálsson, F. (2017). Subglacial volcanic activity above a lateral dyke path during the 2014–2015 Bárdarbunga-Holuhraun rifting episode, Iceland. *Bulletin of Volcanology*, *79*(6), 38. https://doi.org/10.1007/s00445-017-1122-z

Ritter, M. C. (2012). Analogue and numerical modelling of dyke propagation in stratovolcanoes effects of rock mechanical properties and layer thicknesses, (MS thesis). Göttingen, Germany: Department of Structural Geology and Geodynamics, University of Göttingen.

Ritter, M. C., Acocella, V., Ruch, J., & Philipp, S. L. (2013). Conditions and threshold for magma transfer in the layered upper crust: Insights from experimental models. *Geophysical Research Letters*, *40*, 6043–6047. https://doi.org/10.1002/2013GL058199

Rivalta, E. (2010). Evidence that coupling to magma chambers controls the volume history and velocity of laterally propagating intrusions. *Journal of Geophysical Research*, *115*, B07203. https://doi.org/10.1029/2009JB006922

Rivalta, E., Bottinger, M., & Dahm, T. (2005). Buoyancy-driven fracture ascent: Experiments in layered gelatine. *Journal of Volcanology and Geothermal Research*, *144*(1-4), 273–285. https://doi.org/10.1016/j.jvolgeores.2004.11.030

Rivalta, E., & Dahm, T. (2006). Acceleration of buoyancy-driven fractures and magmatic dikes beneath the free surface. *Geophysical Journal International*, *166*(3), 1424–1439. https://doi.org/10.1111/j.1365-246X.2006.02962.x

Rivalta, E., Taisne, B., Bunger, A. P., & Katz, R. F. (2015). A review of mechanical models of dike propagation: Schools of thought, results and future directions. *Tectonophysics*, *638*, 1–42. https://doi.org/10.1016/j.tecto.2014.10.003

Rubin, A. M. (1995). Propagation of magma-filled cracks. *Annual Review of Earth and Planetary Sciences*, *23*(1), 287–336. 287–336, doi:https://doi.org/10.1146/annurev.ea.23.050195.001443

Rubin, A. M., & Pollard, D. (1987). Origins of blade like dikes in volcanic rift zones. In R. W. Decker, T. L. Wright, & P. H. Stauffer (Eds.), *Volcanism in Hawaii* (pp. 1449–1470). Reston, VA: United States Geological Survey.

Ryan, M. P. (1987). Elasticity and contractancy of Hawaiian olivine tholeiite and its role in the stability and structural evolution of subcaldera magma reservoirs and rift system. In R. W. Decker, T. L. Wright, & P. H. Stauffer (Eds.), *Volcanism in Hawaii* (pp. 1395–1447). Reston, VA: United States Geological Survey.

Ryan, M. P. (1994). Neutral-buoyancy controlled magma transport and storage in mid-ocean ridge magma reservoirs and their sheeted-dike complex: A summary of basic relationships. In M. P. Ryan (Ed.), *Magmatic systems* (pp. 97–135). San Diego, CA: Academic Press. https://doi.org/10.1016/S0074-6142(09)60094-2

Schuler, J., Greenfield, T., White, R. S., Roecker, S. W., Brandsdóttir, B., Stock, J. M., et al. (2015). Seismic imaging of the shallow crust beneath the Krafla central volcano, NE Iceland. *Journal of Geophysical Research: Solid Earth*, *120*, 7156–7173. https://doi.org/10.1002/2015JB012350.1

Sigmundsson, F., Hooper, A., Hreinsdóttir, S., Vogfjörd, K. S., Ófeigsson, B. G., Heimisson, E. R., et al. (2015). Segmented lateral dyke growth in a rifting event at Bárðarbunga volcanic system, Iceland. *Nature*, *517*(7533), 191–195. https://doi.org/10.1038/nature14111

Taisne, B., & Jaupart, C. (2009). Dike propagation through layered rocks. *Journal of Geophysical Research*, *114*, B09203. https://doi.org/10.1029/2008JB006228

Taisne, B., & Jaupart, C. (2011). Magma expansion and fragmentation in a propagating dyke. *Earth and Planetary Science Letters*, *301*(1-2), 146–152. https://doi.org/10.1016/j.epsl.2010.10.038

Taisne, B., & Tait, S. (2009). Eruption versus intrusion? Arrest of propagation of constant volume, buoyant, liquid-filled cracks in an elastic, brittle host. *Journal of Geophysical Research*, *114*, B06202. https://doi.org/10.1029/2009JB006297

Taisne, B., & Tait, S. (2011). Effect of solidification on a propagating dike. *Journal of Geophysical Research*, *116*, B01206. https://doi.org/10.1029/2009JB007058

Taisne, B., Tait, S., & Jaupart, C. (2011). Conditions for the arrest of a vertical propagating dyke. *Bulletin of Volcanology*, *73*(2), 191–204. https://doi.org/10.1007/s00445-010-0440-1

Takada, A. (1990). Experimental study on propagation of liquid-filled crack in gelatin: Shape and velocity in hydrostatic stress condition. *Journal of Geophysical Research*, *95*, 8471–8481. https://doi.org/10.1029/JB095iB06p08471

Townsend, M. R., Pollard, D. D., & Smith, R. P. (2017). Mechanical models for dikes: A third school of thought. *Tectonophysics*, *703-704*, 98–118. https://doi.org/10.1016/j.tecto.2017.03.008

Turcotte, D. L., & Schubert, G. (2014). *Geodynamics*. Cambridge, England: Cambridge University Press.

Urbani, S., Acocella, V., Rivalta, E., & Corbi, F. (2017). Propagation and arrest of dikes under topography: Models applied to the 2014 Bardarbunga (Iceland) rifting event. *Geophysical Research Letters*, *44*, 6692–6701. https://doi.org/10.1002/2017GL073130

Urbani, S., Acocella, V., & Rivalta, E. (2018). Supplementary material for analogue experiments on lateral versus vertical dike propagation. GFZ Data Services. http://doi.org/10.5880/fidgeo.2018.012

Watanabe, T., Masuyama, T., Nagaoka, K., & Tahara, T. (2002). Analog experiments on magma-filled cracks: Competition between external stresses and internal pressure. *Earth, Planets and Space*, *54*(12), 1247–1261. https://doi.org/10.1186/BF03352453

Wright, T. J., Sigmundsson, F., Pagli, C., Belachew, M., Hamling, I. J., Brandsdóttir, B., et al. (2012). Geophysical constraints on the dynamics of spreading centres from rifting episodes on land. *Nature Geoscience*, *5*(4), 242–250. https://doi.org/10.1038/ngeo1428

Ziv, A., Rubin, A. M., & Agnon, A. (2000). Stability of dike intrusion along preexisting fractures. *Journal of Geophysical Research*, *105*, 5947–5961. https://doi.org/10.1029/1999JB900410

Zucca, J. J., Hill, D. P., & Kovach, R. L. (1982). Crustal structure of Mauna Loa Volcano, Hawaii, from seismic refraction and gravity data. *Bulletin of the Seismological Society of America*, *72*, 1535–1550.